# Effects of cascade-induced dislocation structures on the long-term microstructural evolution in tungsten

## Bonny, G.

2020-08

# Effects of cascade-induced dislocation structures on the long-term microstructural evolution in tungsten

G. Bonny[1][1], N. Castin[1], A. Bakaev[1], A.E. Sand[2], D. Terentyev[1]

[1] SCK CEN, Nuclear Materials Science Institute, Boeretang 200, B-2400 Mol, Belgium

[2] Department of Physics, University of Helsinki, P.O. Box 43, FIe00014 Helsinki, Finland

### *Abstract*

In recent years, a number of systematic investigations of high-energy collision cascades in tungsten employing advanced defect analysis tools have shown that interstitial clusters can form complex non-planar dislocation structures. These structures are sessile in nature and may potentially have a strong impact on the long-term evolution of the radiation microstructure. To clarify this aspect, we selected several representative primary damage states of cascades debris and performed annealing simulations using molecular dynamics (MD). We found that immobile complexes of non-planar dislocation structures (CDS) evolve into glissile and planar shaped ½<111> loops with an activation energy of ~1.5 eV. The CDS objects were implemented in an object kinetic Monte Carlo (OKMC) model accounting for the event of transformation into 1-D migrating loops, following the MD data. OKMC was then used to investigate the impact of the transformation event (and the associated activation energy) on the evolution of the microstructure.

## 1. Introduction

Tungsten (W) is the material of choice as armor of plasma-facing components in fusion devices such as the international thermonuclear experimental reactor (ITER) and the demonstration power station (DEMO) [1, 2]. Under fusion operational conditions, the effects of 14 MeV neutron irradiation are detrimental to the physical (e.g. thermal conductivity) and mechanical properties (e.g. fracture toughness) of W. It is well known that irradiation by fast neutrons shifts the ductile-to-brittle transition temperature up, which beyond a certain fluence leads to the formation of cracks under cyclic heat load of the component [3]. In the presently

---

[1] Corresponding author (G. Bonny), gbonny@sckcen.be ; giovanni.bonny@gmail.com

explored water cooled mono-block design of the divertor, the cracks may lead to a loss of vacuum accident, thereby exposing the environment to toxic and volatile tungsten tri-oxide particles that clearly pose a safety threat.

The degradation of the mechanical properties is linked to the irradiation induced microstructure, consisting essentially of nanometric dislocation loops, voids and precipitates of transmutation products [4]. Large efforts are dedicated to develop predictive tools to model the evolution of the radiation microstructure under the target fusion-irradiation conditions, such as, fluence, flux and temperature [5].

One of such tools is the object kinetic Monte Carlo (OKMC) approach, which is capable of predicting the irradiation-induced microstructure under various irradiation conditions [6-11]. A crucial input parameter for an OKMC tool is the primary damage state, i.e., the cascade debris induced by the primary knock-on atom (PKA), created as the result of elastic interaction with a high-energy neutron or ion. In a standard OKMC code, self-interstitial atom (SIA) clusters are represented by planar circular disks, representative of a dislocation loop. In bulk W, the majority of experimentally observed loops are of ½<111> type [11-13], which are highly mobile [14]. Therefore, in the standard OKMC models for W, only mobile ½<111> loops are considered [6, 7, 9].

In recent years, systematic investigations of high PKA energy (~200 keV) collision cascades in W [15, 16], coupled with advanced defect analysis tools [17-19] have shown that in-cascade created interstitial clusters can form complex non-planar dislocation structures (CDS). These structures consist of several junctions of ½<111> and <100> dislocation segments. Although these dislocation structures represent a minority of the SIA defect populations (~7% of all SIA clusters from a database 1-200 keV cascade debris), they are sessile and may therefore influence the long-term microstructural evolution.

Clearly, these CDS do not fit the standard OKMC description of SIA clusters as disk-like 1-D migrating loops. Therefore, the present work is dedicated to the assessment of the impact of these sessile dislocation structures on the long-term evolution of the irradiation microstructure within an OKMC framework.

The objectives of the present study are twofold: i) to investigate cascade annealing at high temperature using molecular dynamics (MD) to study the evolution of the CDS with respect to their potential transformation into regular loops; ii) assess the consequences of the formation (and transformation) of sessile dislocation structures on the long term evolution of the radiation microstructure.

As will be presented below, the MD simulations show that pathways exists for the CDS to evolve into standard planar ½<111> loops on the MD time scale. Based on this result, a class of sessile dislocation loops is introduced into the OKMC developed in [7, 11]. This class is then assigned an activation energy to evolve into a mobile planar ½<111> loop based on the MD simulations. The impact of this new class of objects on the irradiation-induced microstructure under the most severe irradiation conditions is assessed.

## 2. Methods

Cascade annealing was performed using molecular dynamics (MD) simulations with the large-scale atomic/molecular massively parallel simulator (LAMMPS) [20]. A data base, consisting of 10 separate cascade debris for a 200 keV PKA energy, generated according to the procedure described in [15], was considered for annealing. Besides ½<111> loops, these debris contained complex non-planar dislocation structures (CDS).

The simulation boxes used in the cascade simulations consist of up to 13 million atoms. To reduce the simulation time, the extreme coordinates of the defects were identified and the simulation box was reduced such that all defects were included within a box with an additional 3 nm of pristine W on every side. This procedure resulted in simulation boxes containing up to 1.3 million atoms.

The MD simulations were performed in ($N,p,T$) ensemble at zero pressure using free surfaces in all directions. As such, mobile defects that escape from the cascade volume do not return through periodic boundaries and do not interfere with the evolution of the cascade debris. The simulations were performed at 1500 K for up to 5 ns with a time step of 1 fs.

To assess the effect of interatomic potential, three different W potentials were considered: i) 'EAM2' potential developed by Marinica et al. [21]; ii) the potential developed by Ackland and Thetford [22, 23]; and iii) the potential developed by Chen et al. [24].

The object kinetic Monte Carlo (OKMC) simulations were performed using the model developed in [7]. In short, the model considers the following objects: interstitial atoms, vacancies, ½<111> loops, and voids. These objects are allowed to diffuse, grow, dissociate, annihilate and get trapped by carbon impurities. At every OKMC step, an object can be annihilated at sinks with corresponding strength based on the initial microstructure, i.e., dislocation density and grain size.

At each irradiation event, a cascade debris configuration is chosen at random from the cascade database and introduced at a random spot in the OKMC box. Thereby the PKA

spectrum corresponding to the irradiation type, ion or neutron irradiation is respected (see [11-13] for a detailed description). It is noted that possible effects of cascade overlap are not accounted for in the present model.

In the above model, an additional class of immobile objects was implemented representing the sessile CDS. These immobile objects were allowed to transform into glissile ½<111> loops with an activation energy derived from the MD simulations.

Thus, two mechanisms impede the motion of loops in the employed model: i) trapping of loops by single C impurities present in the W matrix; and ii) CDS introduced via the source term. The trapping energy between a loop and single C impurities is derived from density functional theory (DFT) computations. A linear regression based on the binding energy between a single C atom and SIA cluster containing 1, 7, 19 and 37 SIAs (forming small prismatic loops) [25] was implemented. For loops containing more than 50 SIAs, the trapping energy is chosen to saturate to 2.1 eV, which is the static binding energy between a single C atom and an edge dislocation (ED) [26]. The latter serves as limiting case for a loop of infinite size.

We mention that the model assumptions used here are different from our previous work [7]. In our previous work, we demonstrated that the model predictions (loop/void size/density) are in best agreement with experimental data when stronger traps than single C impurities are defined. These were so-called "C-originated traps", and were assumed to be compounds constituted of C atoms and vacancies. The parametric study performed in [7] concluded that their optimal value for the saturation point was as high as 2.5 eV.

In the present work, we only consider the interaction between loops and single C impurities, thereby fully relying on the DFT-evaluated binding energies. These binding energies are lower than in the previous model, but closer to CDS activation energy (see further). Thus, the present conservative implementation promotes the competition between trapping by C and unfaulting of CDS.

The OKMC model was applied to simulate the ion and neutron irradiation experiments similar to the ones in [13].

## 3. Results

### 3.1. Molecular Dynamics

Ten different cascade debris from 200 keV cascades initiated in random directions were annealed for up to 5 ns at 1500 K. A representative example (the most complex CDS is visualized) is shown in Fig. 1. The initial state and outcome after cascade annealing for all considered cascade debris are summarized in **Appendix A**. The initial state (the outcome of the cascade) is characterized by three sessile CDS consisting of junctions of ½<111> and <100> segments.
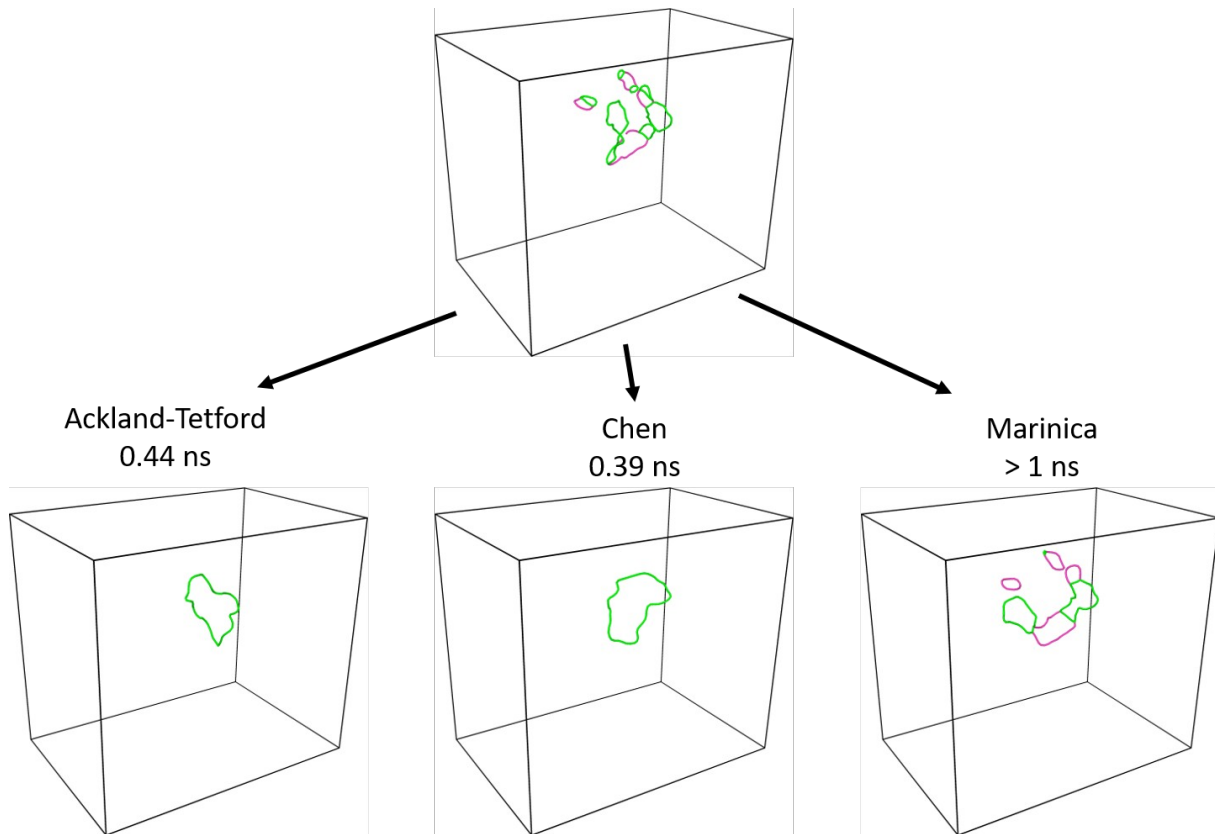


Fig. 1 − Evolution of the primary damage state after cascade annealing at 1500 K using the Ackland-Thetford, Chen and Marinica potentials [21, 23, 24]. The visualizations are the result of the DXA analysis implemented in Ovito [17-19]. For clarity, only the dislocation segments are visualized. The green and magenta lines indicate ½<111> and <100> dislocation segments, respectively.

For both the Ackland-Thetford and Chen potentials, the CDS evolve into nearly planar glissile ½<111> loops within a similar timespan (~0.4 ns). Note that within this timespan, the two smaller CDS already converted into mobile ½<111> loops that migrated outside the visualized box volume.

For the Marinica potential, on the other hand, the CDS remain sessile. In fact, the two smaller CDS evolved into sessile <100> loops. These observations are consistent with the choice of potentials. Indeed, while both Ackland-Thetford and Chen potentials stabilize ½<111> loops over <100> loops, the opposite is true for the Marinica potential [24]. The latter is a known shortcoming of the Marinica potential and explains the essentially different outcome of the simulation [24].

Except for the Marinica potential, the CDS in all investigated cascade debris evolved into glissile ½<111> loops within the MD time scale using either Ackland-Thetford or Chen potentials, similar to the example case described above.

The unfaulting of the CDS is influenced by stress fields, vacancy/interstitial fluxes introduced by the surrounding cascade debris, as well as by spontaneous, thermally activated, transformation [27, 28]. However, given the complexity of the cascade debris, it is impossible to separate the individual contributions of each mentioned mechanism. Therefore, the presented results are qualitative, rather than quantitative. They foremost show the existence of pathways for CDS to evolve into glissile ½<111> loops within the MD time scale. Nevertheless, to provide an indication of the magnitude of the transformation barrier, an approximate analysis is provided in the following.

The transition rate, $\Gamma$, associated to the unfaulting of CDS is given as,

$$\Gamma = v_0 \exp\left(\frac{-F_a}{kT}\right),  \tag{1}$$

with $F_a$ the activation free energy associated to the CDS unfaulting, $v_0$ an attempt frequency, $T$ the temperature and $k$ the Boltzmann constant. Here $v_0 = 8 \times 10^{12} \, s^{-1}$ was chosen, consistent with the Debeye temperature of W, i.e., 400 K.

For each CDS in the cascade debris, we recorded the time, $\Delta t$, for the CDS to evolve into a ½<111> loop. The probability of counting one transition event (CDS unfaulting) within $\Delta t$ for a specific $F_a$ is given by the Poisson distribution,

$$p(\Delta t, F_a) = \Gamma \, \Delta t \exp(-\Gamma \, \Delta t).  \tag{2}$$

From this probability, we can derive the probability of the free energy barrier $F_a$, given the transition at time $\Delta t$ as,

$$p(F_a|\Delta t) = \frac{p(\Delta t, F_a)}{\int\limits_0^\infty p(\Delta t, F_a) dF_a} = \frac{\Gamma \Delta t \exp(-\Gamma \Delta t)}{kT[1 - \exp(-\nu_0 \Delta t)]}. \tag{3}$$

From this distribution, the average $\langle F_a \rangle$ and standard deviation $\sqrt{\langle (F_a - \langle F_a \rangle)^2 \rangle}$ are obtained via numerical integration. It is noted that in the present work the analysis is based on a single transition rate. For more accurate statistics, ~10 independent MD simulations are necessary, as discussed in-depth in [29].

Since the simulations were performed at a single temperature ($T = 1500 K$), we introduce an error resulting from the entropic contribution to the activation barrier. If the entropy is assumed to be of the order $k$, the resulting error is $kT \approx 0.13 eV$. Thus, the total error on $\langle F_a \rangle$ is estimated as,

$$\delta F_a = \sqrt{\langle (F_a - \langle F_a \rangle)^2 \rangle} + kT. \tag{4}$$

The resulting $\langle F_a \rangle$ derived from the MD simulations with Ackland-Thetford and Chen potentials for all studied cases is summarized in Fig. 2, as a function of loop size (number of SIAs, $N_{SIA}$, in the cluster). The scatter in values resulting from Ackland-Tethford and Chen potentials give a measure of the induced uncertainties by the use of the different interatomic potentials. For the Marinica potential, no meaningful results could be obtained due to the wrong loop stability.
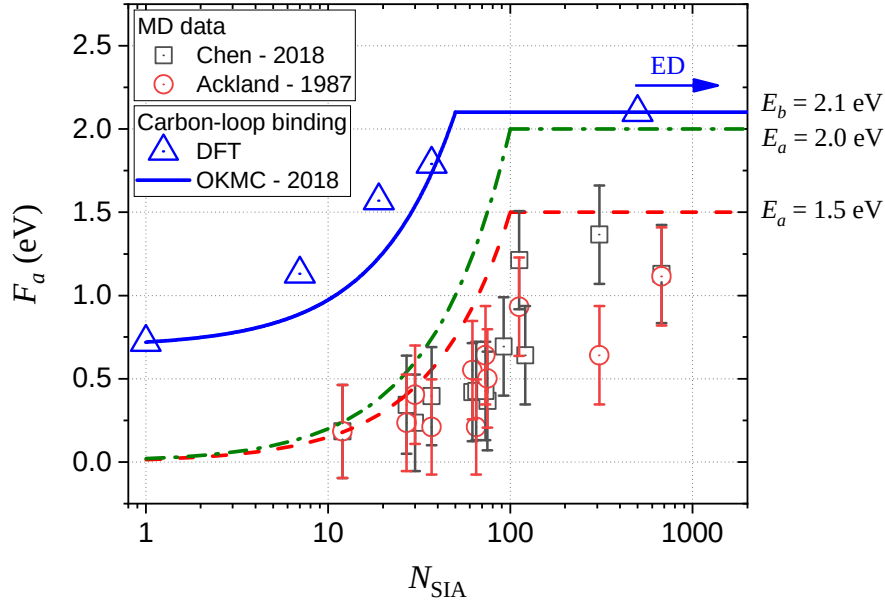
Fig. 2 – Activation free energy, $\langle F_a \rangle$, as a function of loop size, $N_{SIA}$, obtained from MD simulations using the Ackland-Thetford and Chen potentials. The limiting cases for $F_a$ as implemented in the OKMC are indicated by the green dash dot and red dashed lines. The blue line indicates the binding energy between loop and C-traps as implemented in the OKMC model. Density functional theory (DFT) values for the C-loop and C-edge dislocation (ED) binding energy are added to the figure [11, 26].

We observe that despite the large scatter between the individual CDS and potentials, both potentials show the same trends. The $\langle F_a \rangle$ increases quasi linearly with $N_{SIA}$ and seems to saturate from $N_{SIA} \approx 100$. As a conservative estimate, the upper bound of $F_a \approx 1.5\,\text{eV}$ encompasses all MD data.

## 3.2. Object Kinetic Monte Carlo

Given the MD results, immobile CDS objects with given activation free energy to transform into mobile ½<111> loops are implemented in our OKMC code [7, 11]. This process is schematically illustrated in Fig. 3. A competing process present in the OKMC model is the trapping of ½<111> loops at C impurities, thereby immobilizing the loops with an activation energy equal to its binding energy to the trap.

MD picture                                                    OKMC picture
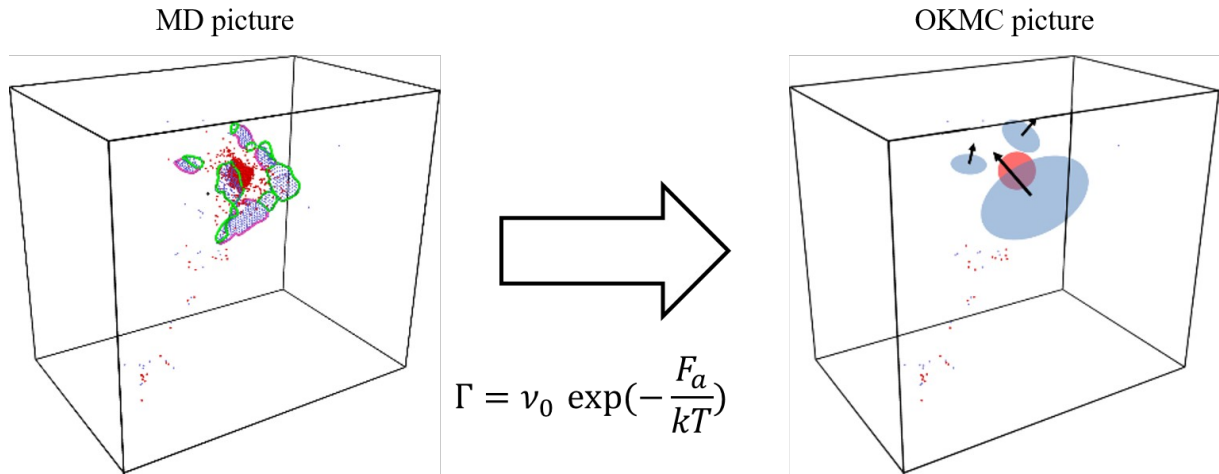
$$\Gamma = \nu_0 \, \exp(-\frac{F_a}{kT})$$

Fig. 3 – Schematic representation of how (CDS containing) cascade debris obtained in MD are converted to idealized OKMC objects consisting of spherical voids and circular ½<111> loops. In the MD box, both Wigner Seitz and dislocation analyses are added. Blue shades represent interstitial (clusters) and red shades represent vacancy (clusters). The green and magenta lines indicate ½<111> and <100> dislocation segments, respectively.

To assess the difference in activation energy between both processes, the binding energy of a ½<111> loop and C impurity as implemented in the OKMC model is added to Fig. 2. The binding energy increases linearly from 0.72 eV, i.e., the binding between C and a single SIA [26], up to 2.1 eV (corresponding to the binding between a C trap and edge dislocation [26]) for $N_{SIA} = 50$, after which the binding energy saturates [25]. Thus, given the limited occurrence of CDS and compared to the $F_a$ due to C trapping, the introduction of CDS is not expected to have a large impact on the evolution of the irradiation microstructure.

To test the actual impact of CDS and its sensitivity to $F_a$, we performed two sets of OKMC simulations for the limiting cases $F_a = 1.5\,eV$ and $F_a = 2.0\,eV$, consistent with the MD results, and a value close to the saturation binding energy between loop and C trap, respectively.

As limiting cases for the C trap concentration, we chose $C_C$ = 20 and 200 appm [11]. The value of 200 appm is a typical value for the C content in ITER specified W grades [30]. As not all C is necessarily dissolved in the matrix, i.e., it is also distributed at the dislocation network and grain boundaries, it was varied by an order of magnitude down to 20 appm.

To maximize the potential impact of the CDS objects, we considered an ion irradiation experiment with 18 MeV self-ions at 400 °C and 800 °C, respectively. The temperature of

400 °C is the lower temperature limit in the divertor mono-block concept, while 800 °C corresponds to the temperature of peak swelling [31]; hence large changes in the radiation microstructure are expected.

These choices are expected to maximize the potential impact because: i) the high energy 18 MeV self-ions ensure a non-negligible fraction of 200 keV PKA events, thus maximizing the number of introduced CDS; ii) the high dose rate, typically $10^{-4}$ dpa/s, compared to ~$10^{-7}$ dpa/s for most neutron irradiation test facilities, minimizes the annealing time between successive irradiation events; iii) the irradiation temperature is chosen just below long range vacancy migration (400 °C) and at peak swelling (800 °C).

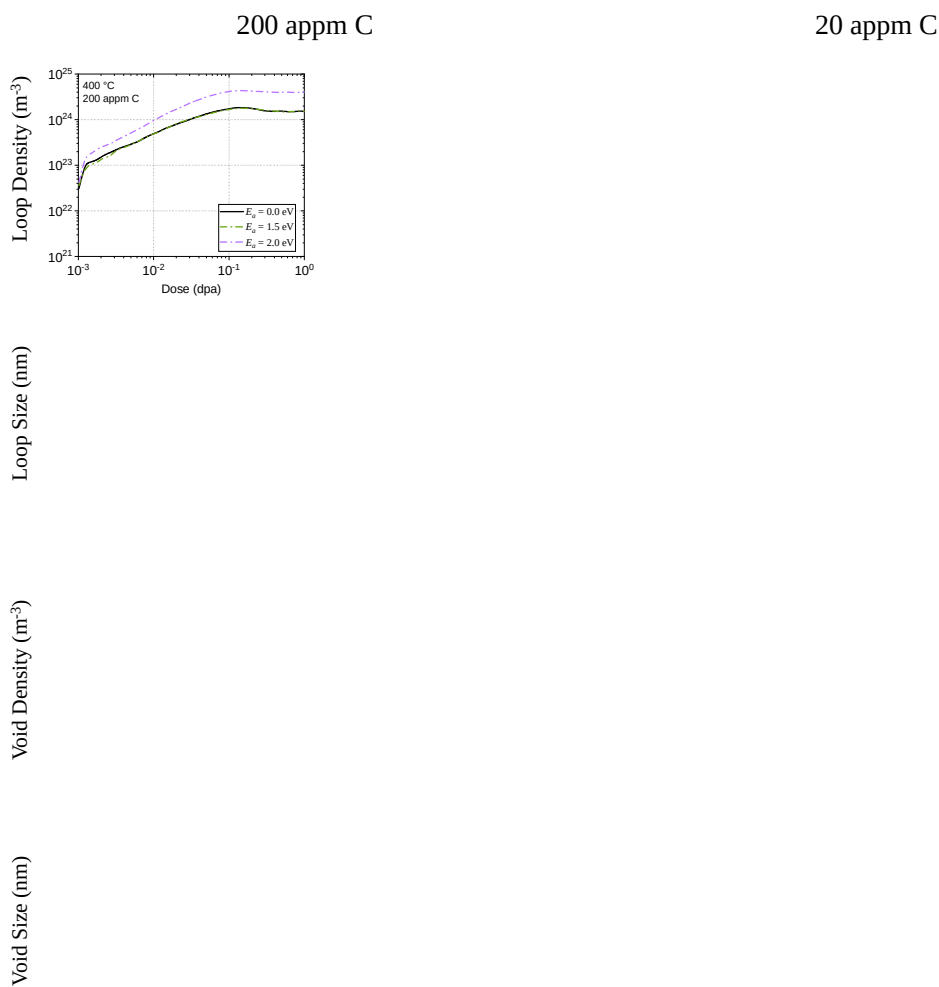200 appm C                    20 appm C



Fig. 4 – Evolution of the OKMC simulated ion irradiation-induced microstructure in terms of average void/loop size and density for all simulated conditions.

Thus, a total of four different cases were simulated, summarized in Fig. 4. An in depth discussion comparing loop/void size/density to experiments is provided in [7]. In the scope of the present paper, where the model was adapted to promote the competition between C-loop trapping and CDS unfaulting (see **section 2**), we focus on the effect of CDS with different values for $F_a$ on the radiation microstructure. For all investigated conditions, we observe that void size and density are unaffected by the introduction of CDS. The loop size and density, on the other hand, are affected only at 400 °C for $F_a = 2.0\,eV$. For the latter conditions, the loop density increases and loop size decreases compared to the case without CDS. With decreasing C content, this effect becomes more pronounced. These observations highlight the competition between effective loop trapping by C impurities and the unfaulting of CDS into mobile ½<111> loops.

To substantiate this statement further, the density of sessile CDS and sessile C-trapped loops is plotted in Fig. 5. Sessile configurations can be realized either as a CDS, or C-trapping of an otherwise mobile loop. As such, only an effect on the results is expected if the density of CDS loops is larger or similar in magnitude to the density of C-trapped loops. As shown in Fig. 5, this is indeed the case at 400 °C for $F_a = 2.0\,eV$. For $F_a = 1.5\,eV$, on the other hand, the density of C-trapped loops is significantly higher than the density of sessile CDS and therefore CDS have no impact on the total loop density.

Thus, given that $F_a$ is significantly lower than the binding energy between a loop and a C impurity, the effect of trapping by C shadows the effect of CDS, except when the concentration of C is low enough, or $F_a$ is large enough. Considering that the effective concentration of C is always higher than 20 appm above 400 °C (see detailed discussions in Ref. [6, 7, 11]) and $F_a = 1.5\,eV$ (see MD simulations), we do not expect CDS to have a significant impact on the OKMC model predictions.
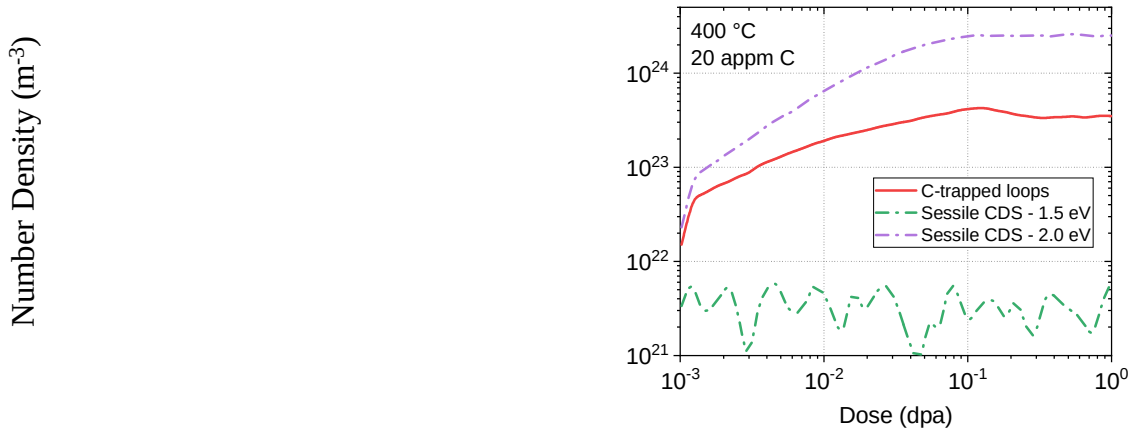
Fig. 5 – Comparison of the number density of sessile CDS and C-trapped loops at 400 °C.

For completeness, the same simulations were performed for neutron irradiation conditions, i.e., a typical dose rate of $10^{-7}$ dpa/s and PKA spectrum for a fast fission reactor. The same temperature, C content and CDS activation free energy range were explored as for the 18 MeV self-ion irradiation. The results of this exercise are added to **Appendix B**. These simulations show that the CDS have no impact on the irradiation-induced microstructure, even for $F_a = 2.0\,eV$. As expected, the softer PKA spectrum and lower dose rate, compared to 18 MeV self-ion irradiation, limit the density of sessile CDS.

## 4. Conclusive Remarks

In this work, we performed post-cascade annealing on several 200 keV cascade debris using molecular dynamics (MD) simulations and followed the structural transformation of the sessile dislocation defects formed after the collision phase of a cascade. We found that immobile complex non-planar dislocation structures (CDS) evolve into glissile planar ½<111> loops within the MD time scale. Assuming an Arrhenius type of transformation process and measuring the transformation time at fixed temperature, we deduced a conservative estimate of the activation free energy of ~1.5 eV for the sessile set of junctions to be converted into a glissile ½<111> loop.

Based on the MD data, immobile CDS objects with given activation energy to transform into mobile ½<111> loops were implemented in an object kinetic Monte Carlo (OKMC) model as a new set of objects. Subsequently the code was used to simulate 18 MeV self-ion irradiation as well as neutron irradiation at 400-800 °C. Besides considering the

information obtained from MD simulations, the activation free energy was varied to explore its impact.

For ion irradiation, it was found that CDS with an activation free energy consistent with the MD results have no impact on the evolution of the radiation microstructure. However, an activation free energy close to the C-loop binding energy can yield an impact for low C content and low irradiation temperature.

Under neutron irradiation conditions, on the other hand, which allow for longer annealing times between cascade events due to the significantly lower dose rate and softer PKA spectrum, the CDS were shown to have no impact on the results for any of the investigated conditions.

Despite this conclusion, some critical remarks are in place. Although the present MD study provides evidence that the CDS evolve towards planar ½<111> loops, the activation free energy associated to this process was only roughly estimated. Large scatter in the derived activation energy is observed due to the presence of several radiation defects, i.e., vacancies and interstitial (clusters) that interact with the CDS. These interactions may lead to a variety of competing processes with different activation energy, such as, dislocation climb by absorption of point defects, elastic interactions with radiation defects, etc.

## Acknowledgements

## Data Availability

The raw/processed data are available from the corresponding author on reasonable request.

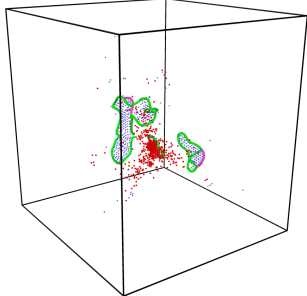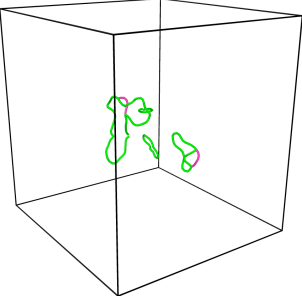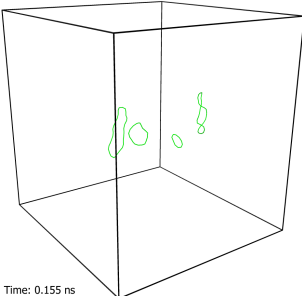## Appendix A: Cascade Ageing via Molecular Dynamics

In the present appendix, all cascade debris considered for the molecular dynamics (MD) simulations are presented. The cascade debris are the result of 200 keV cascade simulations [15, 16].
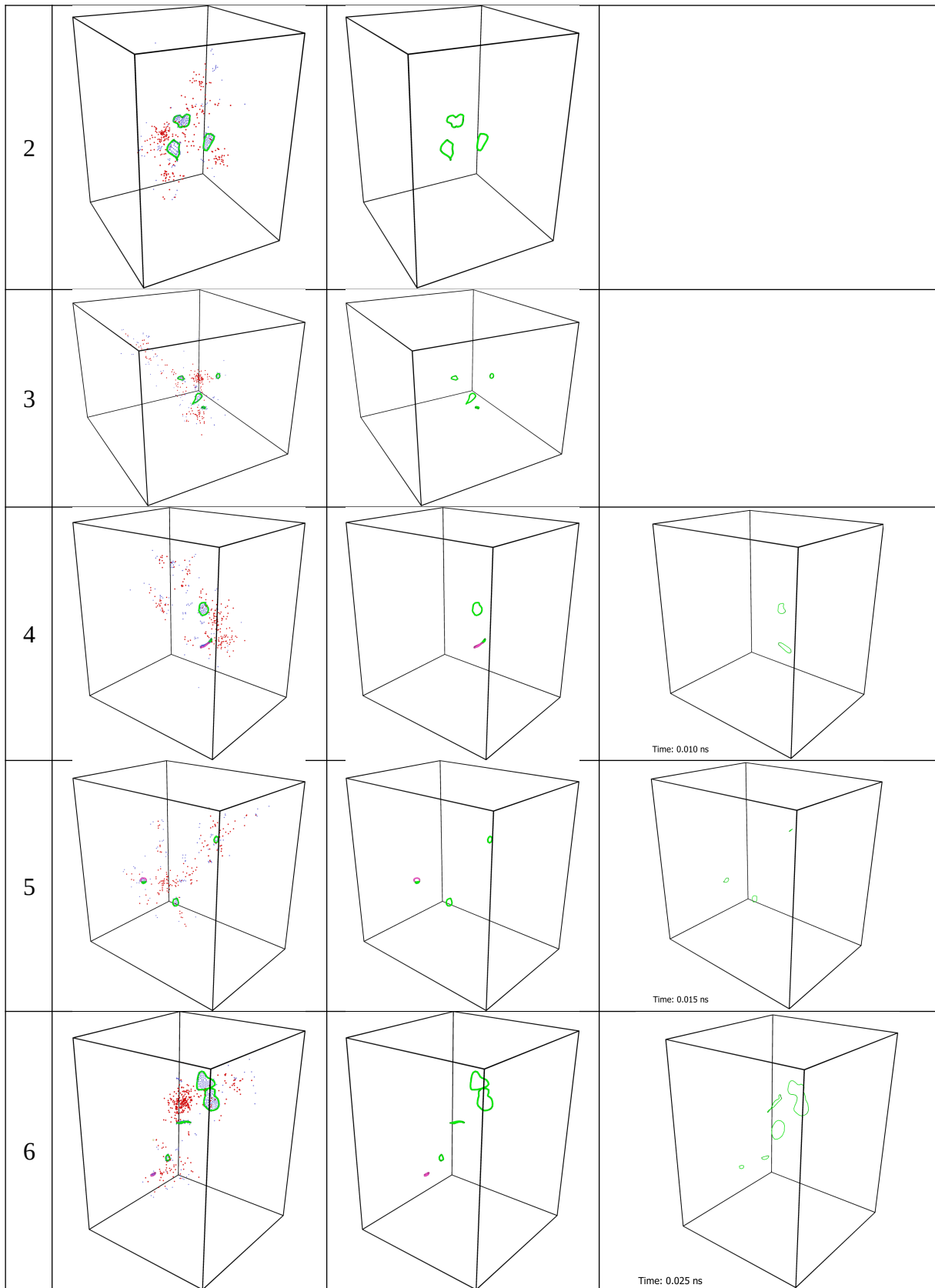
**Table A1** summarizes all configurations considered for cascade annealing. The initial configurations are characterized by both Wigner-Seitz (WS) analysis and dislocation analysis (DXA), while the final configurations were visualized using DXA only, for the sake of clarity. In the plots, ½<111> dislocation segments are indicated in green, while <100> dislocation segments are indicated in magenta. Vacancies are indicated in red, while interstitial atoms are indicated in blue.

In the initial frames, the CDS are characterized by triple junctions of <100> and/or ½<111> segments. In configuration 6, also a small <100> loop was present. Clearly, all CDS (including <100> loops) evolve into ½<111> loops, all free of junctions and therefore glissile, within the MD time scale.

We note that for configurations 2 and 3 do not contain any CDS. Hence, no cascade annealing was applied.

**Table A1** – All configurations considered for cascade annealing. The initial configurations are characterized by both Wigner-Seitz (WS) analysis and dislocation analysis (DXA), while the final configurations were visualized using DXA only, for the sake of clarity. In the plots, ½<111> dislocation segments are indicated in green, while <100> dislocation segments are indicated in magenta. Vacancies are indicated in red, while interstitial atoms are indicated in blue.
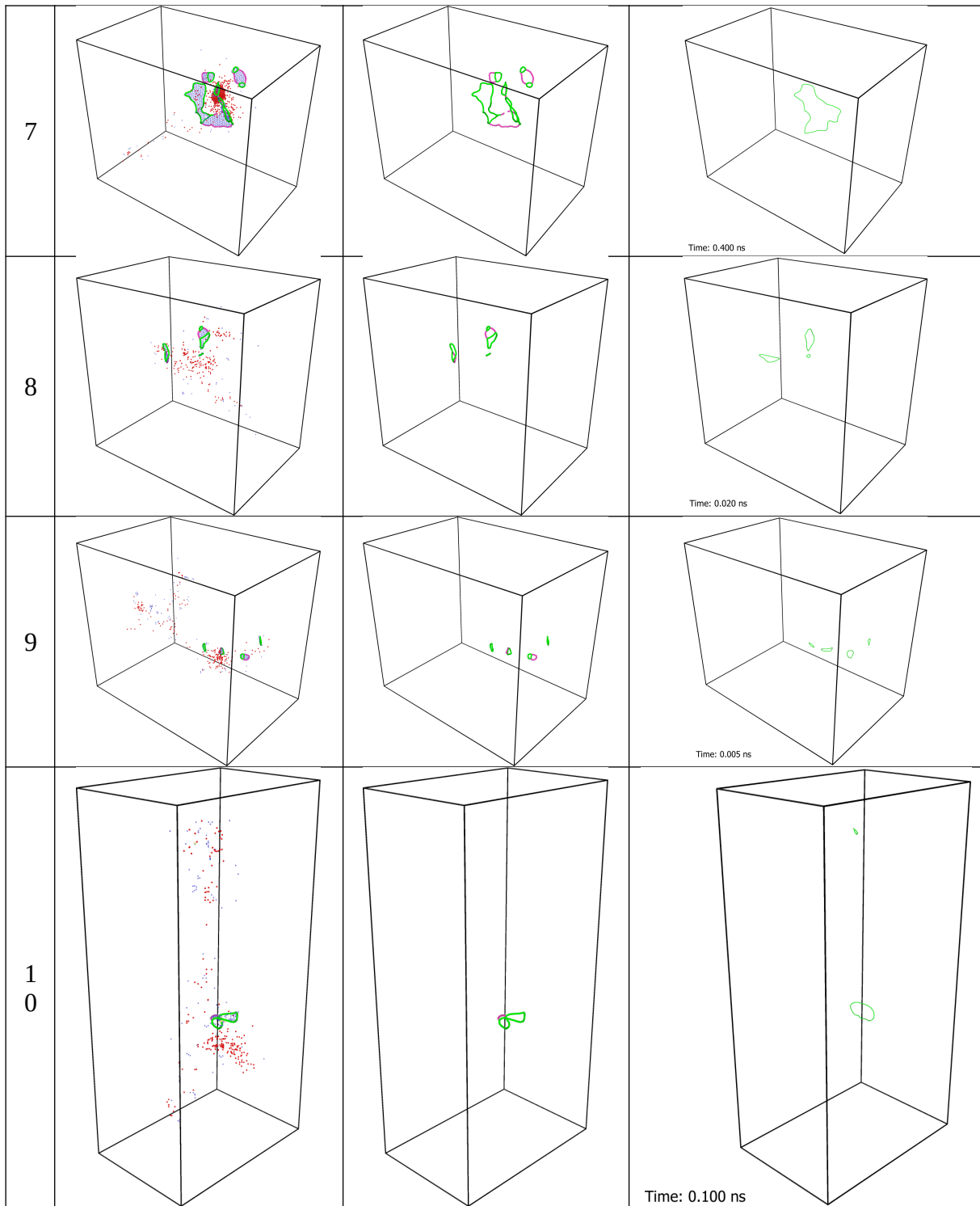
| # | Initial | | Final |
|---|---------|---|-------|
|   | WS+DXA | DXA | DXA |
| 1 | | | Time: 0.155 ns |

| | | | |
|---|---|---|---|
| 2 | | | 15 |
| 3 | | | |
| 4 | | | Time: 0.010 ns |
| 5 | | | Time: 0.015 ns |
| 6 | | | Time: 0.025 ns |

Time: 0.400 ns

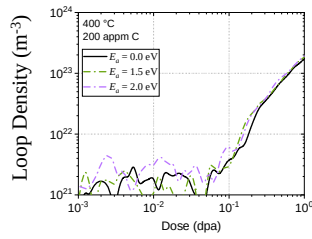Time: 0.020 ns

Time: 0.005 ns

Time: 0.100 ns

## Appendix B: Neutron Irradiation Conditions

The simulation of neutron irradiation for the four different conditions, i.e., 400-800 °C and 20-200 appm C, is summarized in Fig. B1. For all investigated conditions, we observe that void/loop size and density are unaffected by the introduction of CDS.

200 appm C                                    20 appm C



Loop Density (m⁻³)

Loop Size (nm)

Void Density (m⁻³)

Void Size (nm)

Fig. B1 – Evolution of the OKMC simulated neutron-irradiation induced microstructure in terms of average void/loop size and density for all simulated conditions.

**References**

[1] S.J. Zinkle, Physics of Plasmas, 12 (2005) 1-8.
[2] S. Matsuda, K. Tobita, Journal of Nuclear Science and Technology, 50 (2013) 321-345.
[3] G. Pintsuk, I. Bobin-Vastra, S. Constans, P. Gavila, M. Rödig, B. Riccardi, Fusion Eng Des, 88 (2013) 1858-1861.
[4] T. Tanno, M. Fukuda, S. Nogami, A. Hasegawa, MATERIALS TRANSACTIONS, 52 (2011) 1447-1451.
[5] G. Pintsuk, E. Diegele, S.L. Dudarev, M. Gorley, J. Henry, J. Reiser, M. Rieth, Fusion Eng Des, 146 (2019) 1300-1307.
[6] N. Castin, A. Bakaev, G. Bonny, A.E. Sand, L. Malerba, D. Terentyev, Journal of Nuclear Materials, 493 (2017) 280-293.
[7] N. Castin, G. Bonny, A. Bakaev, C.J. Ortiz, A.E. Sand, D. Terentyev, Journal of Nuclear Materials, 500 (2018) 15-25.
[8] F. Jiménez, C.J. Ortiz, Computational Materials Science, 113 (2016) 178-186.
[9] C.S. Becquart, M.F. Barthe, A. De Backer, Phys Scr T, T145 (2011) 014048.

[10] C.J. Ortiz, A. Souidi, C.S. Becquart, C. Domain, M. Hou, Radiat Eff Defects Solids, 169 (2014) 592-602.

[11] N. Castin, A. Dubinko, G. Bonny, A. Bakaev, J. Likonen, A. De Backer, A.E. Sand, K. Heinola, D. Terentyev, Journal of Nuclear Materials, 527 (2019) 151808.

[12] W. Van Renterghem, I. Uytdenhouwen, Journal of Nuclear Materials, 477 (2016) 77-84.

[13] T. Hwang, M. Fukuda, S. Nogami, A. Hasegawa, H. Usami, K. Yabuuchi, K. Ozawa, H. Tanigawa, Nucl. Mater. Energy, 9 (2016) 430-435.

[14] G. Bonny, N. Castin, A. Bakaev, D. Terentyev, Computational Materials Science, 144 (2018) 355-362.

[15] A.E. Sand, S.L. Dudarev, K. Nordlund, EPL, 103 (2013) 46003.

[16] A.E. Sand, K. Nordlund, S.L. Dudarev, Journal of Nuclear Materials, 455 (2014) 207-211.

[17] A. Stukowski, Modelling and Simulation in Materials Science and Engineering, 18 (2010) 015012.

[18] A. Stukowski, K. Albe, Modelling and Simulation in Materials Science and Engineering, 18 (2010) 085001.

[19] A. Stukowski, Modelling and Simulation in Materials Science and Engineering, 20 (2012) 045021.

[20] S. Plimpton, Journal of Computational Physics, 117 (1995) 1-19.

[21] M.C. Marinica, L. Ventelon, M.R. Gilbert, L. Proville, S.L. Dudarev, J. Marian, G. Bencteux, F. Willaime, Journal of Physics-Condensed Matter, 25 (2013) 395502.

[22] M.W. Finnis, J.E. Sinclair, Philosophical Magazine A: Physics of Condensed Matter, Structure, Defects and Mechanical Properties, 50 (1984) 45-55.

[23] G.J. Ackland, R. Thetford, Philosophical Magazine A: Physics of Condensed Matter, Structure, Defects and Mechanical Properties, 56 (1987) 15-30.

[24] Y. Chen, Y.-H. Li, N. Gao, H.-B. Zhou, W. Hu, G.-H. Lu, F. Gao, H. Deng, Journal of Nuclear Materials, 502 (2018) 141-153.

[25] A. Bakaev, et al, Manuscript in preparation, (2020).

[26] A. Bakaev, A. Zinovev, D. Terentyev, G. Bonny, C. Yin, N. Castin, Y.A. Mastrikov, E.E. Zhurkin, Journal of Applied Physics, 126 (2019) 075110.

[27] M.A. Puigví, N. de Diego, A. Serra, Y.N. Osetsky, D.J. Bacon, Philosophical Magazine, 87 (2007) 3501-3517.

[28] A. Chartier, M.C. Marinica, Acta Mater., 180 (2019) 141-148.

[29] T.D. Swinburne, D. Perez, Physical Review Materials, 2 (2018) 053802.

[30] See https://www.plansee.com/en/materials/tungsten.html. for "the information on chemical composition of manufactured W grades."

[31] J. Matolich, H. Nahm, J. Moteff, Scripta Metallurgica, 8 (1974) 837-841.